IEEE Access
Multidisciplinary | Rapid Review | Open Access Journal

Received March 20, 2022, accepted March 31, 2022, date of publication April 5, 2022, date of current version April 14, 2022.

Digital Object Identifier 10.1109/ACCESS.2022.3165059

Active-Clamp Flyback Converter as Auxiliary Power-Supply of an 800 V Inductive-Charging System for Electric Vehicles

DARKO Đ. VRAČAR[1,2], (Member, IEEE), AND PREDRAG V. PEJOVIĆ[1], (Senior Member, IEEE)
[1]School of Electrical Engineering, University of Belgrade, 11000 Belgrade, Serbia
[2]BRUSA Elektronik (München) GmbH, 81829 Munich, Germany

Corresponding author: Darko Đ. Vračar (darko.vracar@brusa.biz)

This work was supported by BRUSA Elektronik (München) GmbH, Munich, Germany (www.brusa.biz).

ABSTRACT Investigation of active-clamped flyback (ACF) dc-dc converter 57 W used as the auxiliary power-supply (APS) of an inductive-charging system (ICS) is presented. The ACF was supplied from variable-dc-link 800 V which was challenge for its design. Anyway, some findings are applicable to any ACF. An overview of ACF control ICs is presented revealing that only two vendors have appropriate devices for ICS. The key-parts' choice and suggestion of new features targeting ACF in this emerging-application are given. Striving for high switching-frequency in ICS is not needed due to large safety-distances of transformer. Measured ''*maximum-efficiency vs. magnetizing-inductance*'' graph showed that extremes are reached for 400 μH. It was based on four transformers with manually-optimized resonant-tanks. Measurements of ''*circulating-power losses vs. input-voltage*'' are compared for several transformers. Those losses are in the range of few watts and increase with input-voltage. Measurements of ''bandwidth, phase-margin and gain-margin vs. input-power'', for different input-voltages, are discussed. Those quantities were changeable with load and input-voltage as expected. The short-circuit behavior is analyzed showing that usage of the hybrid-clamp with multi-mode control-ICs is mandatory. Finally, comparison with conventional flyback and quasi-resonant flyback converters showed that both are ≈23 % cheaper, occupy ≈11 % less board-space, and have similar or higher efficiencies. The reason for such efficiency is that ACF circulating-power losses were high as well as dc-voltage-conversion-ratio. Although this is a drawback, for an APS the efficiency is not the key-parameter as long as there are no thermal problems. Moreover, as ACF converter is known for having less EMI-problems that could be the key-advantage for this application. But problem is not-enough electronic components on the market that are suitable for ICS.

INDEX TERMS Active-clamped flyback, auxiliary power-supply, control, dc-dc converter, inductive charging-system, quasi-resonant flyback.

NOMENCLATURE

ACF	active-clamped flyback.
ACM	active-clamping mode.
APS	auxiliary power-supply.
CCM	continuous conduction-mode.
DCM	discontinuous conduction-mode.
EMI	electro-magnetic interference.
EV	electric vehicle.
FET	field-effect transistor.
GM	gain margin.
HDCIV	higher-dc-input-voltage.
HV	high-voltage.
IC	integrated circuit.
ICS	inductive charging-system.
IPT	inductive power-transfer.
PES	power-electronic system.
PM	phase margin.
PWM	pulse-width modulation.
QRF	quasi-resonant flyback.
RCD	resistor-capacitor-diode.
SiC	Silicon-carbide.

The associate editor coordinating the review of this manuscript and approving it for publication was Alfeu J. Sguarezi Filho.

SMD surface-mounted devices.
SW switching node.
ZVS zero-voltage switching.

I. INTRODUCTION

In recent years we are witnessing increasing interest in inductive power-transfer (IPT) and wireless charging of electric vehicles (EV) [1]–[6]. The research focus was mainly on power-conversion stages, efficiency improvements, compensation (i.e. tuning), control, and coil design. To our best knowledge no one was concerned with auxiliary power-supplies (APS) of such systems so far. From first authors' experience APS are often overlooked and taken for granted in many other projects. Engineers are usually focused on the ''big picture'' (i.e. whole system) hence forget that if APS is not working properly then the system will not work as well. For single-phase supplied IPT systems there are no challenges regarding APS since there are plenty of proven standard-solutions used in other (industrial) products. But, for the three-phase supplied IPT systems, where dc link is higher than 450 V, depending on the chosen topology, one might face some challenges that will be studied in this work.

This paper presents evaluation of active-clamped flyback (ACF) dc-dc converter 57 W used as the APS of a commercial wireless inductive-charging system (ICS) for EV. The ICS is supplied from three-phase grid. Note that the ACF is used as APS of primary (i.e. ground located) side of a wireless ICS. The term ICS is used in *BRUSA Elektronik AG* [7], instead of IPT, so it will be used in this paper as well.

The active-clamped flyback (ACF) dc-dc converter is well known topology [8], [9], and nowadays is popular in power adapter applications [10]–[12]. The analysis and design of the ACF are well explained in [9], [13]–[17]. Moreover, it is worth watching the video [18] too. Only minimum of ACF operation principles will be repeated here for sake of the paper completeness.

In the majority of literature published so far the ACFs were either supplied from rectified single-phase mains or from batteries (<60 V) [19], [20]. Only few papers had ACF with high-output voltage (>450 V) in exotic applications [21], [22].

First two papers that covered ACF usage with higher-dc-input-voltages (HDCIV), i.e. >450 V, were [23], describing the ACF supplied from 800 V variable-dc-link, and [24] covering the ACF supplied from passively-rectified three-phase mains (460–640 V). Both papers [23], [24] had the variable-frequency ACF used as either main or stand-by APS of a wireless ICS for EV, respectively. Main motivators to experiment with ACF in ICS were expectation to achieve high efficiencies—as reported in many papers—and curiosity. However, for the HDCIV case it was seen that ACF has comparable efficiency with conventional flyback dc-dc converter [23], [24]. In experimental section this problem will be further elaborated.

This paper builds on the work started in [23]. Its main focus will be on ACF—although some comparisons will be provided for conventional flyback converter in discontinuous conduction-mode (DCM) and quasi-resonant flyback (QRF) dc-dc converter as APS for ICS. Note that some evaluations of ACF vs. DCM flyback and ACF vs. QRF, but for different applications, were done in [25] and [19], respectively. In [25] the ACF was a fixed-frequency one and just a table with efficiencies is shown. In [19] the ACF was a high-temperature fixed-frequency one with complementary-switching and comparisons were only on a topological-level. Comparisons in this paper will be focused on price, board-space, and efficiency difference in HDCIV application.

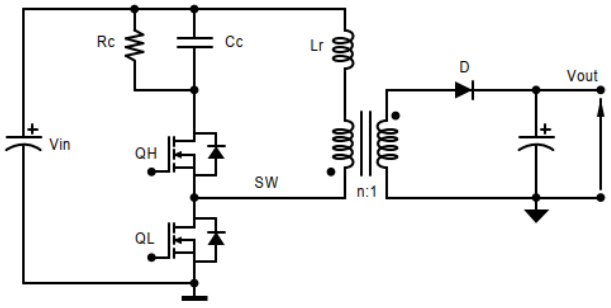

FIGURE 1. The ACF generic schematic.

The ACF generic schematic is shown in Fig. 1. In it V_{in} is voltage of input supply-capacitor (i.e. dc link), QH and QL are high- and low-side switches, respectively; L_r comprises external inductor and leakage inductance, C_c is clamping capacitor, L_m magnetizing inductance, n transformer turns-ratio, D output diode, and V_{out} is the output voltage. The ACF is different than conventional flyback converter in sense that QH is used instead of the clamping diode (which is used in a standard passive RCD snubber). The QH is actively controlled in order to improve efficiency by recycling energy stored in the leakage inductance [23]. In HDCIV applications one has to use external inductor in order to achieve zero-voltage switching (ZVS) of the QL [23], [24].

The general advantages and disadvantages of an ACF in single-phase applications, compared to conventional flyback are listed in [23], [24]. However, it is found that for three-phase input (i.e. HDCIV) application, with the high dc-voltage-conversion-ratio (>80), the efficiency is comparable or even lower than the conventional flyback dc-dc converter and that usage of (external) inductor is mandatory [23], [24]. Additional drawbacks are need for cooling of that inductor as well as higher price and occupied board-space. The bottleneck for wider ACF usage in ICS is lack of appropriate electronic components on the market. However, as ACF is known for having less EMI-related problems [26] that could be the key-advantage for this application.

A. PAPER GOALS AND GAPS IN LITERATURE

The goals of writing this paper were sharing of the experience with ACF in HDCIV application, extension of the previous

work [23], [24], and filling-in some gaps in literature on ACF—which were found during this process.

Note that this paper introduces neither a new topology nor a control strategy, but usage of the known topology (ACF) in an emerging application (i.e. ICS for EV). This brought new insight and challenges related to the ACF design, operation, and control. However, some conclusions will be generally valid for any ACF converter.

In majority of published papers on ACF their authors had kind of custom-made control (analog or digital)—with few exceptions. However, this work was part of a commercial project. Therefore, one had to use off-the-shelf analog-control IC—which was partially a constraint for this study.

Having reviewed more than 70 papers—directly or indirectly related to the ACF—several gaps in literature are identified. Those gaps, independent on input supply-voltage or application, are:

- Possibility that efficiency of an ACF might be equal or even lower than a conventional flyback dc-dc converter was not elaborated in detail. It was briefly announced in [14] and [15] as possibility. Otherwise, in majority of papers the efficiency was reported as much higher. Similar problem was also mentioned when first author talked with a design engineer from another company.
- There was no "*maximum efficiency vs.* L_m" graph—showing that only one combination of L_m-n-L_r-C_c can give maximum ACF efficiency, i.e. optimal design. The L_m stands for magnetizing inductance, n is turns ratio, L_r resonant inductance, and C_c is clamping capacitance.
- The circulating-power losses were not studied for complementary-switching ACF in DCM. In addition, there was no "*circulating-power losses vs. input dc voltage*" graph presented so far. In [20] the complementary-switching continuous conduction-mode (CCM) ACF was briefly studied. Some theoretical work is done for non-complementary switching ACF in [14], for DCM and CCM, as well as in [27] for the CCM case.
- Regarding ACF control, the plots of "(f_c, *PM, GM) vs. input-power*" were missing. The f_c stands for bandwidth (or cross-over frequency), PM for phase-margin, and GM for gain-margin. Typically, other authors would just plot whole Bode diagrams, for few operating points, to justify their approach.

Note that critical analysis of some references will be done on-the-fly throughout the paper—i.e. not in this section.

B. PAPER CONTRIBUTIONS

This paper, together with [23] and [24], presents unique and original contributions to the ACF in the HDCIV application. Key contributions of this paper are summarized below.

1) For a given ACF specification, including transformer, there are values of magnetizing inductance, turns-ratio and resonant-tank parameters that give minimum losses—hence maximum converter-efficiency. This is experimentally confirmed by evaluating four transformers with manually (i.e. trial-and-error) optimized resonant-tank parameters (i.e. L_r-C_c). The appropriate graph and curve-fit formula are provided and explained.

2) The "c*irculating-power losses vs. input dc-voltage*" graphs, for six transformers, are presented for the first time. These losses are in the range of few watts and increase with input-voltage as expected.

3) Components' choice and challenges in HDCIV applications are explained in detail. Moreover, suggestion of features for the new ones is done too. In HDCIV applications usage of external inductor is a must in order to achieve ZVS of the QL [23]. The challenges related to components were choice of high-side driver and its bootstrap diode, semiconductor switches, and inductor. Problem is that there are only single-source components on the market that can fulfill demanding requirements for ICS. Moreover, the required bootstrap diode in small SMD package still does not exist on the market.

Other challenges were manual optimization of clamping circuit with external inductor (i.e. resonant tank), board-space constraints, and construction of the transformer (by external vendors).

In addition, the design guideline is provided for a case with two load-ranges and two input-voltage ranges. This is unique design-case for an ACF reported so far.

4) Only two analog control ICs for ACF, with integrated high-voltage startup (up to 700 V), are available on the market. However, in 800 V applications the external high-voltage (HV) start-up circuit must be implemented too. In addition, measured switching-node voltage, used for ZVS control, has to be scaled to a safe level of <700 V. Hence, there is a definitive need, in ICS application, to create analog control IC for ACF that can work with input dc voltages up to 950 V. Suggestions of new IC's features, firstly made in [23], are updated in this study.

In this application, aiming for high switching-frequency, as in many of published papers on ACF, is not needed. The reason is requirements for high clearance and creepage safety-distances that required the bobbin to be large enough.

5) The used ACF analog control-ICs are multi-mode ones. This means that, at lighter load, they operate in either pulse- skipping mode or with disabled active-clamping mode (ACM), i.e. like conventional flyback dc-dc converter in DCM. Therefore, usage of a hybrid-clamp (i.e. resistor in parallel to the clamping capacitor) is mandatory with multi-mode control ICs in order to avoid damage of the circuit. Notes on how to design it are given in the paper. In [28], [29] the term hybrid-clamp is introduced, but for different (low-voltage) applications.

Short-circuit behavior of ACF is evaluated for the first time in literature. This is the additional reason for usage of the hybrid-clamp in HDCIV application. Otherwise one might get very high SW node voltage (up to 1500 V).

6) Comparisons between ACF and conventional DCM flyback as well as QRF dc-dc converters are made using the same specification, switches (SiC FETs), transformer,

and secondary-side components. Result is that both the conventional DCM flyback and QRF are ≈23 % cheaper and occupy ≈11 % less board-space. In addition, they have higher efficiency than ACF at loads <50 % (for conventional DCM flyback) and at loads <100 % (for QRF). This gives a challenge to the designers for ACF improvement and optimization in HDCIV application. Also, findings 3)–6) are supposed to motivate components' vendors to develop new devices that are targeting HDCIV applications.

7) Bode plots are measured for three input-voltages at 10 different loads. Then bandwidth (f_c), PM, and GM are extracted and plotted versus input-power for the first time. They were changeable with input-voltage and load as expected. In addition, from those plots one can confirm that with only Type-2 compensator (integrator, one pole, and one zero) the ACF converter can be stabilized. In other words, there was no need to go for Type-3 compensator (i.e. two poles, two zeros, and integrator) like in some other papers. The dynamic-load (i.e. step-load change) graphs are shown to verify this approach. It is also found that bandwidth had to be <1/30 of the minimum switching-frequency (f_{sw_min})—contrary to the common suggestions of $f_c < 1/10\, f_{sw\_min}$.

II. BACKGROUND AND DESIGN NOTES

The design considerations for the power stage such as primary switch, transformer, output capacitors, and output rectifiers are similar as for conventional flyback dc-dc converter [14] hence will be omitted. Only specific aspects of the ACF in ICS application will be elaborated here.

A. OVERVIEW OF ACF CONTROL ICs

For APS of any power-electronic system (PES) one needs dedicated (analog) control IC. The APS has two fundamental requirements. It must always start during PES power-on and operate reliably in all operating conditions for the designed lifetime of the PES. The APS efficiency per se is not the key parameter as long as there are no thermal-related problems. In our opinion the key features of any APS are reliability, functionality, protection features, occupied area, and cost. The flyback dc-dc converter is typical and most popular dc-dc converter for APS in either DCM, CCM, self-oscillating, or QRF variant. It is simple, cheap, easy to design; multi-outputs are achieved easily as well as isolation between primary and secondary sides; voltage polarity at outputs can be easily changed too [30], [31]. It can be with primary or secondary regulation; with or without synchronous rectification at outputs.

In this study the ACF is used as an APS of ICS. So far only three vendors are providing dedicated control ICs for ACF, namely: *onsemi* [32], *TI* [33], and *Sillana Semi* [34]. Comparison between them is given in Table 1. Note that *Sillana Semi* has more ACF control ICs than shown here, but all of them have integrated 620 V clamp FET. Hence, that feature made them unsuitable for the HDCIV application.

The chosen IC for ICS APS, due to overall ACF converter simplicity, was NCP1568 [32]. The same device was used in [23], [24] as well. Usage of NCP1568 makes ACF to operate with primary-resonance, secondary-side control, N-type clamp [14], adaptive multi-mode with variable switching-frequency, and complementary-switching in ACM with DCM. That would be the full definition of the ACF in this paper. More info on general principles of such operation of an ACF one can find in [17], [32], and [35].

TABLE 1. Comparison between vendors of ACF control ICs.

Item	*onsemi*	*TI*	*Sillana Semi*
Part number	NCP1568	UCC28780	SZ1130
HV start-up 700 V (built-in)	Yes	Yes	No
Enable signal	Yes	Yes (NTC)	No
FET and GaN ready	Yes	Yes	FET
Max switching frequency	1 MHz	1 MHz	146 kHz
ZVS	Yes	Yes	Yes
Adaptive multi-mode operation	Yes	Yes	Yes
Stand-by mode	Yes	Yes	Yes
External driver needed for the low-side switch	No	Yes	No
Integrated clamp-FET	No	No	Yes
SIMPLIS model available	Yes	Yes	No
Package	TSSOP-16	SOIC-16 WQFN-16	SOIC-16

Two additional devices, NCP1568D [36] and UCC28782 [37], were not available at the time of the ICS-project start. Therefore, they were not considered in the Table 1. In addition, the NCP1568D is still in ''product preview'' phase and UCC28782 is more suitable for ac-dc application. Hence, nothing is missed. Note that *Power Integrations* introduced *ClampZero* family of products recently [38]. But they shall be used together with another product of theirs in single-phase applications. Hence, those devices cannot be used in the HDCIV applications as well.

Note that in literature terms DCM or CCM are used for the ACF operating in ACM as well. This depends on whether magnetizing current is positive all the time (CCM) or goes into negative direction during the off-time (DCM) [14]. But, if the same ACF is operating with disabled clamping-branch, at light or small load, then meaning of DCM is as for the conventional flyback converter in DCM. Hence, in this paper the term DCM will be used for disabled-ACM operation of the ACF whereas both terms ACM and DCM ACM will be used for ACF operating with magnetizing current going into negative.

In addition, please keep in mind that the control ICs, mentioned in this section, use complementary-switching of QL and QH. The non-complementary one is somehow not yet preferred in industry [18]—although with its usage one can achieve higher efficiencies [14], [27].

From [32]–[34] it was evident that the IC manufacturers had in mind applications only in single-phase systems. Suggestions of needed features of the potential ACF control ICs for HDCIV applications were initially given in [23] and will be updated in sub-section II-D including advices for other components as well.

TABLE 2. Specification of auxiliary power supply.

Parameter	Value
Input dc voltage (ICS power transfer)	620–880 V
Input dc voltage (ICS stand-by)	460–640 V
Output 1: regulated voltage	+5.5 V
Output 1: load current	1 A
Output 2: voltage	+5.5 V
Output 2: load current	2.15 A
Output 3: voltage	+22 V
Output 3: load current	1.7 A
Output 4/5: voltage	±11 V
Output 4/5: load current	±40 mA
Output power	57 W
System stand-by power	<10 W
DC voltage-conversion-ratio at 5.5 V	112.7–154.5
Minimum switching frequency, f_{sw_min}	66 kHz

TABLE 3. Specification of transformer.

Parameter	Value
Maximum primary peak-voltage	>960 V
Clearance and creepage distances	>7.9 mm
Turns ratio primary to output 1 & 2	15
Turns ratio primary to output 3	3.75
Turns ratio primary to output 4 & 5	7.5
Core shape and material	ETD29, N87
Magnetizing inductance, L_m	0.6 mH
Max peak primary-current, I_{pri_max}	1.83 A

B. CONVERTER SPECIFICATION

The specification of ACF (and QRF) converter for 800 V application is the same as in [23], and is shown in Table 2. In Table 2, the stand-by input voltage range reflects passively rectified three-phase grid voltage (325–450 V, rms, line-to-line) [23].

Minimum switching-frequency was limited by external resistor (pin *5: RT* [32]) to be around 66 kHz. This is out of specification of NCP1568—default minimum is 100 kHz with some tolerances [32]—but it was approved by *onsemi application team* [39]. As a "rule-of-thumb", the 65 kHz is a typical compromise between size and switching losses [30]. The general design-notes for the NCP1568 are given in [40]. The synchronous rectification at outputs was not used in this design because the ACF was already too complicated. Furthermore, in [11] is claimed that primary-resonance ACF (our case) might have instabilities when using synchronous rectification.

At low load (<10 W), i.e. ICS stand-by mode, this ACF operated like conventional flyback in DCM in order to increase the efficiency. With higher loads, the ACF was operating in the ACM.

In this application another challenge was present. Namely the ACF had two input-voltage ranges (Table 2) with different total loads, and different loading of its outputs. For ICS power-transfer mode the ACF maximum load was estimated to be 57 W with all outputs loaded. Under such conditions the ACF operated in ACM. For a case of ICS stand-by mode, where only ancillary functions are active, maximum load was estimated to be up to 10 W. In addition, in that condition, one +5.5 V output and the +22 V one were not loaded at all. In that scenario the ACF operated with disabled-ACM, i.e. like conventional flyback converter in DCM. Such scenario made the ACF control-design more challenging due to cross-regulation effect. Hence, one had to use Zener-diodes and bleeder resistors to keep output voltages within limits at no load. In vast majority of published papers on ACF the authors had only one output in their prototypes—which was much easier to handle.

C. TRANSFORMER DESIGN AND SPECIFICATION

The input voltage across primary winding of transformer was high as well as the requirements for clearance and creepage safety-distances (Table 3). The safety distances were calculated per *IEC 61558*-1 [41]. To reduce safety distances and equalize temperature-distribution the transformer had to be potted as well. Moreover, five outputs at secondary side were present (Table 2) at two different ground potentials. As a result one had to use ETD29 bobbin—a smallest one for this application [23]. Hence, there were no benefits in going for higher switching frequencies than the chosen one.

It is seen that many researchers were trying to achieve as higher switching frequency as possible in order to reduce the ACF volume. This is justified in typical ACF application as power adapter for consumer electronics' market—which is nowadays the mainstream. However, the ACF with HDCIV used as APS for ICS has completely different requirements for transformer (Table 3). That eliminated the need for further reduction of the transformer bobbin size.

Note that for a flyback dc-dc converter the correct term would be coupled-inductors and not the transformer [18], [20], [23], [24]. In a majority of literature and daily use in engineering departments those coupled-inductors are often called transformer so such term will be used here too [23], [24]. However, for the ACF operating in DCM ACM, the magnetizing current is going into negative direction thus flux-cancelation effect happens [10]. Hence, for such an ACF the term transformer is acceptable.

In Fig. 2 the "*magnetizing inductance vs. current*" curve is depicted for the used transformer. The transformer was constructed per Table 3 by a sub-contractor. This means that all construction details are not known to us. General challenge with custom-designed magnetic parts is long lead-time of 7–11 weeks. Hence careful planning of tasks is essential. In Fig. 2 one can notice at which primary current the transformer saturation happens and how it looks like. During operation at 620 V the peak primary-current is 1.83 A which corresponds to magnetizing inductance of 515 μH. This is on knee of the curve in Fig. 2 and at start of the saturation, but still acceptable. Even at higher operating temperature,

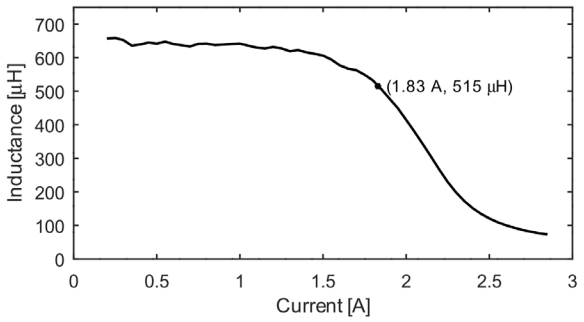

FIGURE 2. The "*magnetizing inductance vs. primary current*" curve for transformer 0.6 mH measured at room temperature. This is what the 57 W ACF experiences in real operation.

when the curve would be shifted to the left, i.e. magnetizing inductance would be lower at 1.83 A, there is still enough margin (down to 400 μH). A design on the edge, such as this one, assures optimal utilization of the magnetic material [24]. More info on the measurement method of the "*magnetizing inductance vs. current*" characteristic one can find in [24].

The ACF magnetizing inductance is chosen as

$$L_m < 0.95 \cdot \min(L_{msb}, L_{mpt}) \tag{1}$$

where L_{msb} and L_{mpt} are magnetizing inductances for ICS stand-by (*sb*) and power-transfer (*pt*) modes, respectively, and 0.95 is a tolerance-correction factor. Inductances are calculated per modified expression from [33]

$$L_{mx} = \frac{D_{\max x}^2 \cdot V_{in\min x}^2 \cdot \eta_x}{2 \cdot P_{outx} \cdot f_{sw\_min}} \tag{2}$$

where x denotes *sb* or *pt* subscripts, D_{max} is max duty-cycle (16 % or 12 %), V_{inmin} is minimum input dc voltage (460 V or 620 V), η assumed maximum efficiency (70 % or 85 %), P_{outx} total output-power (10 W or 57 W), and f_{sw_min} is minimum switching-frequency (66 kHz). The numeric values for L_{msb} and L_{mpt} were 3.44 mH and 0.66 mH, respectively. Hence, the L_m is chosen to be 0.6 mH.

Additionally, in [24] we saw that the leakage inductance is not constant and that it is linearly dependent on primary current. Hence that effect shall be accounted for during any converter design. In this design measured leakage inductance was lower than 9 μH (i.e. <1.5 % L_m). Otherwise, if it were higher, then cross-regulation effect would cause the non-regulated outputs to have much higher voltages at lighter loads.

Note that some of the results in experimental section will be given for ACF with different transformers. Those transformers had similar specification to the one in Table 3 except that magnetizing inductances and (sometimes) turn-ratios were different. More info will be given in IV-D.

Also, consider that in [42] it is emphasized that magnetics optimization is a key to improving overall efficiency of any converter. In this study choice of transformer specification is created manually, i.e. no usage of an optimization algorithm. Moreover, as already said, the construction of transformers is done by sub-contractor companies. Hence, some parameters and their design process are not known to us.

D. CHOICE OF KEY COMPONENTS

Here some practical aspects of components' choice, their features, and availability will be covered. It turned out that only one part, per component category, was commercially available. That is to say, the key-parts (e.g. control IC, power switch, half-bridge driver, bootstrap diode, and inductor) are all single-sourced. That is not desired for the mass-production.

The switching node (SW) in Fig. 1 could go up to 1350 V at light load in DCM (i.e. operation with disabled-ACM). Hence low-side and high-side switches had to be 1700 V rated. Best choice was SiC FET [43] in terms of lower losses and price versus standard high-voltage Si MOSFETs.

Further challenges were choice of high-side driver, and related bootstrap-diode. It is decided to use half-bridge driver with 1500 V isolation, and bootstrap circuit, for driving both switches. With such approach it was ensured that there is enough dead-time so that shoot-through was avoided. The bootstrap diode in SMD (smaller) package (e.g. SMA) has to be rated for 1500 V, have forward voltage-drop <1.25 V, and reverse-recovery time <75 ns (i.e. ultra-fast recovery characteristics). But such a diode still does not exist on the market. Hence, in this design, the 1300 V one was used. Other available diodes (≥1500 V) were either standard-recovery ones or with forward voltage-drop in range 3–6 V—which was not acceptable. Experiments with such sloppy diodes (or bad-chosen driver) always led to destruction of the ACF when operating at voltages >800 V.

Last challenge was choice of external inductor for ZVS. In this ICS application it had to be a SMD one with maximum height <8 mm, maximum temperature >125 °C, low dc resistance (<0.15 Ω), and minimum 2 A rated. The only one part fulfilled those requirements. Moreover, it was the hottest part as well—hence its cooling was needed. This is the major drawback of the ACF in this specific application.

Finally, updated suggestions from [23] for features of the potential ACF control ICs targeting HDCIV systems are:

- HV start-up and self-supply to be in 250–950 V dc input voltage range. Reason for 250 V is that the ACF could be used in USA or Japanese markets.
- Minimum switching frequency of 60 kHz for ACM shall be allowed as the default one [23].
- Ensure that end-user can manually set the ACM- or DCM-only modes. Moreover, in multi-mode operation to have clear transition thresholds DCM-ACM and vice versa, i.e. not to be noise sensitive.
- The IC pin, connected to the SW node, to be able to withstand at least 950 V, i.e. avoiding big shifting of the ZVS detection threshold. Ideally, the 1500 V rating would eliminate need for external voltage divider, thus save costs and board-space.

E. HYBRID CLAMP

Introduction and analysis of the hybrid-clamp for ACF was presented in [28] (with resistor) and [29] (with a TVS diode). Additionally, in [44] is claimed that, in stand-by operation, the clamp-operation is not needed since currents are small hence QL peak-voltage too. Note that in those papers the authors used ACF in single-phase input applications.

In standard power-adapter applications, where ACF is supplied from single-phase grid, multi-mode operation shall not be a problem. But, in our application, the SW node could go up to 1350 V at light-load (i.e. with disabled-ACM). Therefore, usage of the hybrid-clamp was a must. It was decided to do it with resistors. Additional reason for using the hybrid-clamp is protection of ACF primary-side during short-circuits at its outputs. More on that topic will be covered in the sub-section IV-I.

In a standard ACF there is always some huge resistor (1–10 MΩ) for discharge of the clamping capacitor after power-off and for its protection in transients [18], [23], [24]. This has nothing to do with the hybrid-clamp approach because for it one needs resistance in the "kΩ" range.

In order to properly choose clamping resistor one needs to consider that clamping capacitor is chosen per other criteria, i.e. for ACM and not as for the conventional RCD snubber. The DCM clamping-voltage has to be higher than the active-clamping one. This ensures that ACF with hybrid-clamp does not have additional power losses in the ACM. In our case clamping resistor was chosen to be 300 kΩ.

F. CLAMPING CAPACITANCE

In literature several formulas are found on how to calculate value of the clamping capacitance C_c for ACF in DCM ACM mode [8], [33], [40], [45]. They give different results to each other and are shown in (3)–(6). Some of the parameters in (3)–(6) are provided in Table 2 and Table 3, whereas V_F is 0.3 V (voltage-drop on output Schottky diodes) and f_{sw_max} is 68 kHz. The inductance L_r comprises 100 μH external inductor and 8 μH leakage inductance. Minimum and maximum duty-cycles, in ICS power-transfer mode, were 9 % and 12 %, respectively. The (3) (equation *21* in [40]) had a small mistake, but, despite correction, still gives too high value for the clamping capacitor (357 nF). From (4) [33] one gets better result (66 nF). Finally, from (5) and (6), that are adapted from [8] and [45], one can calculate minimum (42 nF) and maximum (166 nF) values, respectively.

$$C_{clamp\_onsemi} = \frac{(1 - D_{\min})^2}{0.5 \cdot f_{sw\_\min}^2 \cdot L_r \cdot \pi^2} \tag{3}$$

$$C_{clamp\_TI} = \frac{1}{L_r} \cdot \left[\frac{L_m \cdot I_{pri\_\max}}{1.5 \cdot \pi \cdot n \cdot (V_{out} + V_F)} \right]^2 \tag{4}$$

$$C_{clamp\_\min} = \frac{(1 - D_{\min})^2}{4 \cdot f_{sw\_\max}^2 \cdot L_r \cdot \pi^2} \tag{5}$$

$$C_{clamp\_\max} = \frac{(1 - D_{\max})^2}{f_{sw\_\min}^2 \cdot L_r \cdot \pi^2} \tag{6}$$

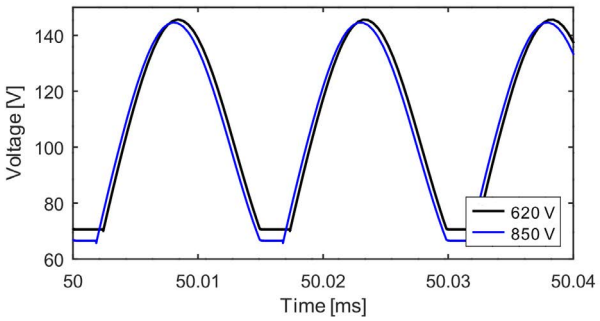

FIGURE 3. The voltage of clamping capacitor for ACF with 57 W load. Maximum at 620 V input was 145.6 V and at 850 V input was 144.6 V.

Hence, for this application, it is found experimentally that C_c of 88 nF and L_r of 108 μH give highest ACF efficiency with L_m of 0.6 mH and n of 15. Those results fell within calculated range from (5) and (6)—which confirmed correctness of that approach. Lesson learned is that one cannot fully rely on the calculations but has to experiment in the lab as well. In this case that was not a big effort since experiments are done for 66 nF, 88 nF and 110 nF capacitances with 68 μH and 100 μH inductors. In ICS project, one had to use capacitor 22 nF for other reasons. Hence, costs of such a capacitor were low and therefore it was chosen for clamping-circuit as well. One can see that resulting C_c values are just multiplies of 22 nF.

In addition, often in literature, the voltage across clamping capacitor is assumed to be constant, i.e. that capacitance is very big, in order to derive equations easily or make further conclusions. However, in reality the available board-space, safety-distances (clearance and creepage), SMD package size, capacitor-voltage ratings, and costs are limiting factors. In addition, optimal value does not have to be big. That shows that capacitance cannot be assumed to be big enough or even chosen exactly according to calculations. As a result the voltage of clamping-capacitor is very changeable. The simulation example is given in Fig. 3. More info is available in [23], [24]. Furthermore, the captured waveforms are shown in experimental section (Fig. 10 and Fig. 11).

G. NOTES ON ZERO-VOLTAGE SWITCHING

One of the positive features of ACF is having ZVS of the QL, thus reducing its switching losses. In addition—depending on control method and resonant-tank choice—even ZVS of the HS switch is possible to achieve as well [15]. In HDCIV application of ACF, as an APS, one had to use additional inductor in order to achieve ZVS of the QL switch [23], [24]. The ZVS is not only beneficial to efficiency improvements but for reduction of electromagnetic interference (EMI) [26]. Moreover, with good choice of resonant-tank parameters it is possible to achieve zero-current switching of secondary-side diodes too [25], [45]. A good analysis of clamping-capacitance influence is provided in [15] and [16].

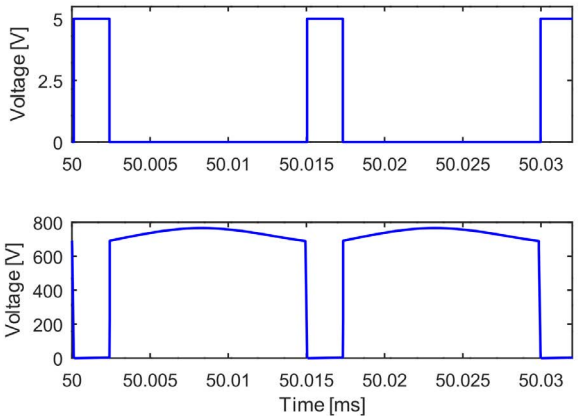

FIGURE 4. The ACF steady-state waveforms at 620 V input and 57 W load in ACM. Upper trace: QL gate-source signal; lower trace: switching node voltage (Vds(QL) = SW).

Due to high SW-node voltage one had to scale its value to <700 V on the control IC input (pin 16: *SW*) [23], [32]. The NCP1568 uses information from this pin for adaptive dead-time control and proprietary ZVS-based frequency-modulation [23]. The scaling of SW pin voltage, with factor of 0.47, meant that the ZVS detection-threshold was shifted from 9.6 V to 20.4 V [23]. The converter's efficiency was not reduced by this action because output capacitance of the SiC FET [43] is lower in the latter case [23].

Note that ACF with NCP1568 operates in DCM ACM. Hence this will have influence on calculation of L_r and C_c. It is known than necessary condition for ZVS of switch QL is that stored energy in lumped leakage-inductance (W_L) has to be higher than the stored energy in lumped parasitic-capacitance (W_C) [8] [9]. Some authors call this relation "energy-balance equation" [15]. At minimum dc input-voltage this is not a problem to achieve since peak current is highest. But, at max dc input-voltage (850 V) the W_C is highest possible whereas the peak primary-current is lowest, hence the W_L too. Therefore, one had to use additional inductor [23], [24].

The lumped parasitic-capacitance at SW node (C_{lump}) consists of output capacitances (C_{oss}) of switches, primary-reflected capacitances of output diodes, and parasitic capacitance of primary winding. After evaluating voltage waveform of the SW node by oscilloscope it is found that C_{lump} is around 186 pF. The (resonant) inductance L_r is defined in previous sub-section III-F.

In our case the clamping capacitance is chosen enough big (88 nF) so that resonant period is not finished before QH turns-off (see Fig. 5 and Fig. 7). This means that in energy-balance equation stored energies in both magnetizing and lumped inductances are contributing to the ZVS conditions of QL [15]. The energies in inductances and lumped capacitance are calculated as [15]

$$W_L = 0.5 \cdot L_{lump} \cdot I^2_{clamp(-)} + 0.5 \cdot L_m \cdot I^2_{m(-)} \qquad (7)$$

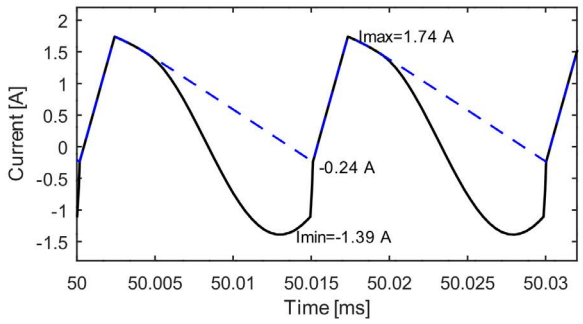

FIGURE 5. The simulated magnetizing (blue dashed line) and primary (black solid line) currents of ACF in steady-state in ACM at 620 V dc input and 57 W load.

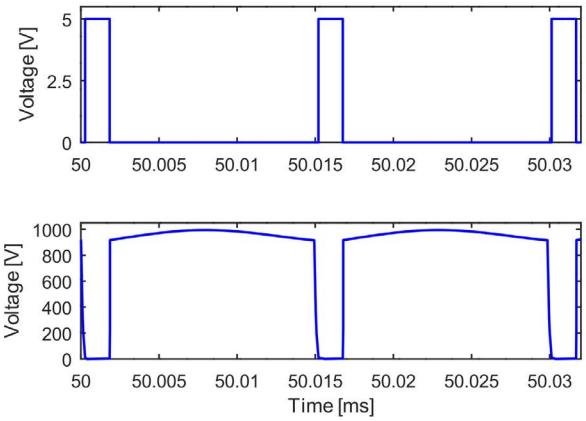

FIGURE 6. The ACF steady-state waveforms at 850 V input and 57 W load in ACM. Upper trace: QL gate-source signal; lower trace: switching node voltage (Vds(QL) = SW).

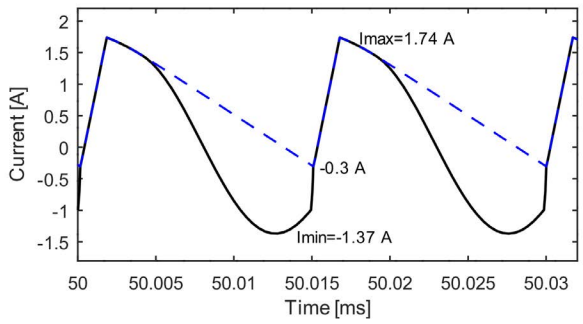

FIGURE 7. The simulated magnetizing (blue dashed line) and primary (black solid line) currents of ACF in steady-state in ACM at 850 V dc input and 57 W load.

and

$$W_C = 0.5 \cdot C_{lump} \cdot V^2_{SW}, \qquad (8)$$

respectively. In (7) and (8), the $I_{m(-)}$ is negative magnetizing current, $I_{clamp(-)}$ is negative clamping current when QH is turned-off, and V_{SW} is the voltage across lumped capacitance (i.e. SW node voltage). Note that in our case the L_r is not negligible, compared to L_m, hence V_{SW} has to be calculated

TABLE 4. Stored energies in resonant tank.

Item	Value
Energy in lumped capacitance at 620 V	47.9 µJ
Energy in lumped capacitance at 850 V	88.8 µJ
Energy in inductances at 620 V (at $I_{clamp(-)}$ −1.12 A)	132.5 µJ
Energy in inductances at 850 V (at $I_{clamp(-)}$ −1.12 A)	150.5 µJ

as

$$V_{SW} = V_{in} + n \cdot V_{out} \cdot \left(1 + \frac{L_r}{L_m}\right). \tag{9}$$

The results are summarized in Table 4. Such a table is, for the first time, presented for an ACF converter. The values for currents are taken from Fig. 5 and Fig. 7. Note that value of $I_{clamp(-)}$ is not the absolute-minimum one, like in [15], but at instant when QH is turned-off—which was more realistic and gave a bit lower value for energy in leakage inductance. From Table 4 one can conclude that chosen values satisfy prerequisites for the ZVS operation for QL. This is confirmed by simulations and experiments as well.

III. SIMULATION RESULTS

Simulation of 57 W ACF operation was done in Simplis [46] due to the NCP1568 model availability and fast simulation speed. More info on the used models one can find in [23] and [24]. The standard parts from SIMPLIS library were used in simulation model of the resonant-tank. The simulations of ACF at 460 V and 640 V input voltages are not presented because the waveforms are similar to the ones of a conventional flyback dc-dc converter in DCM. In following text only operation in ACM is evaluated.

A. OPERATION AT 620 V DC INPUT VOLTAGE

The ACF simulation waveforms of gate-source and drain-source voltages, at 620 V input and rated load, are shown in Fig. 4 [23]. One can see that the active-clamping is working as expected with ZVS for QL. The maximum drain-source voltage of QL was ≈ 766 V.

In Fig. 5 one can see magnetizing and primary currents [23]. In ACF operating in DCM ACM, the magnetizing current (i.e. primary current) has to go into negative direction in order to discharge the lumped capacitance of the SW node—thus ensuring ZVS turn-on for the QL. In Fig. 5 one can see that the resonant period is not finished before high-side switch is turned-off. This is result of design (choice) of the resonant-tank parameters and has influence on efficiency [15], [24].

B. OPERATION AT 850 V DC INPUT VOLTAGE

The ACF simulation waveforms of gate-source and drain-source voltages, at 850 V input and rated load, are shown in Fig. 6 [23].

In Fig. 7 one can see magnetizing and primary currents [23]. Comments of the figures are similar as for the 620 V case. The maximum drain-source voltage of QL was ≈ 995 V. When comparing Fig. 5 and Fig. 7 one sees that extreme values of primary (clamping) currents are almost the same—only negative values of magnetizing currents are slightly different.

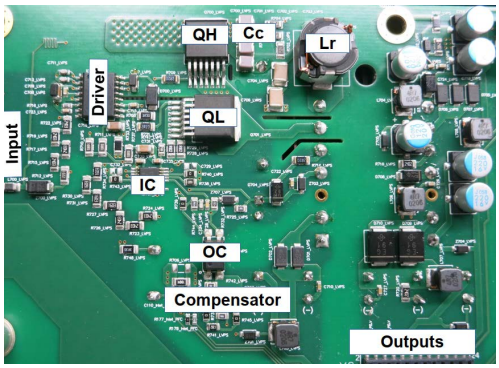

FIGURE 8. The 57 W ACF implemented in system (top view).

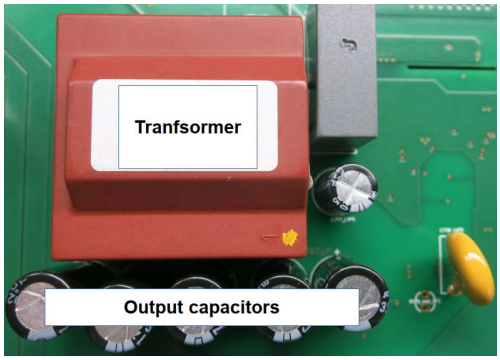

FIGURE 9. The 57 W ACF implemented in system (bottom view).

IV. EXPERIMENTAL RESULTS AND DISCUSSION

The ACF, as specified in Table 2, was built and tested. The implementation photos are shown in Fig. 8 and Fig. 9.

The legend of the oscilloscope waveforms in this section is as follows: **CH1** (yellow; 1 A/div; primary current), **CH2** (green; 200 V/div; drain-source voltage), **CH3** (blue; 5 V/div; gate-source voltage), and **CH4** (red; 50–200 V/div; voltage of the clamping capacitor).

Note that majority of the results presented in this section are actually taken on a demo-board—not in the system itself (i.e. ICS). Such approach was more convenient and safe. The photo of the 57 W ACF demo-board is provided in [23].

A. OPERATION IN ICS POWER TRANSFER MODE

The measured waveforms of gate-source and drain-source voltages at 620 V input and rated load are given in Fig. 10. In it one can see that the active-clamping is working as it should with ZVS for QL. Moreover, those results are matched with the simulation results in Fig. 4.

The measurements of clamping-capacitor's voltage and primary current at 620 V are provided in Fig. 10 as well.

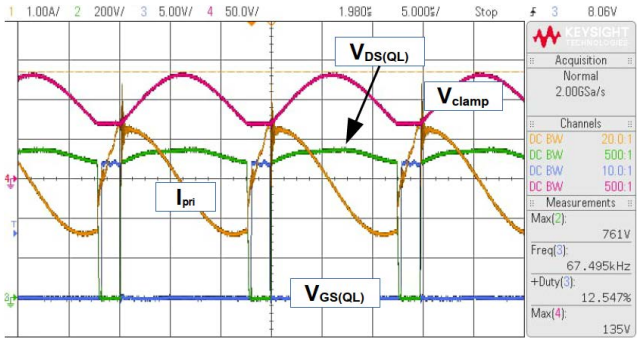

FIGURE 10. The 57 W ACF operating in ACM at 620 V and rated load; V_{clamp} max 134.7 V.

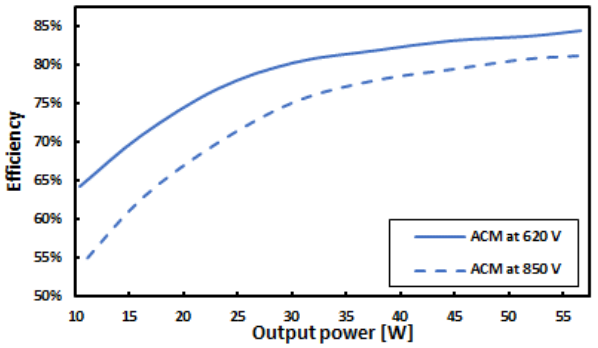

FIGURE 12. The 57 W ACF efficiency curves in ACM measured on a demo-board.

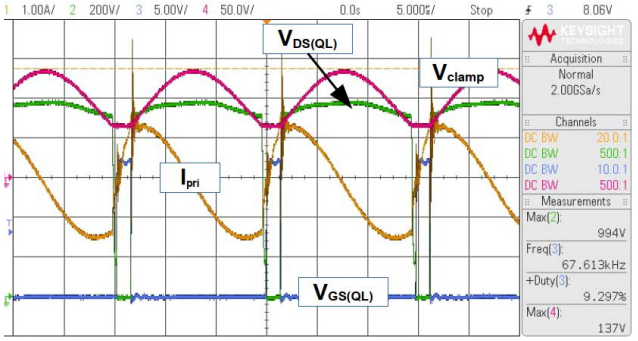

FIGURE 11. The 57 W ACF operating in ACM at 850 V and rated load; V_{clamp} max 136.7 V.

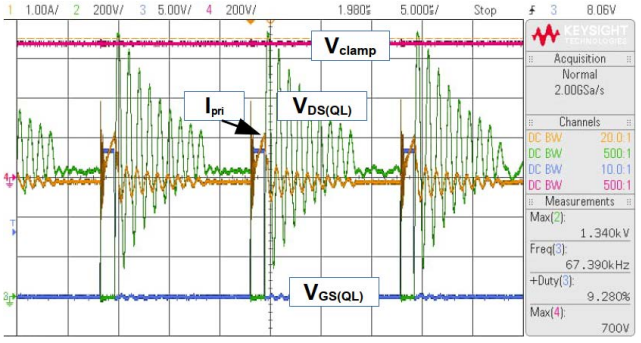

FIGURE 13. The 57 W ACF waveforms at 640 V and 10.5 W (light load; no ACM)) without hybrid-clamp. The max drain-source voltage (i.e. SW node) was 1340 V.

One can notice that maximum voltage of clamping capacitor is $\approx$ 11 V lower than the simulated one (Fig. 3). This is good because it is on a side of safety. In Fig. 10 one can see that there was no saturation of the transformer. Moreover, deviations of primary current extremes (Fig. 5 vs. Fig. 10) are acceptable. The ringing in commutations of QL and QH were inevitable although layout was done carefully.

The measured waveforms of gate-source and drain-source voltages at 850 V input and rated load are given in Fig. 11. In it one can see that the active-clamping is working as it should with ZVS for QL. Moreover, those results are matched with the simulation results in Fig. 6—except for partial ZVS of QL turn-on in Fig. 11. This effect was happening at loads >75 % and is acceptable when referring to discussion in [15] (i.e. that partial ZVS can reduce overall losses a bit). Moreover, although energy in inductances at 850 V (Table 4) was high enough it seems that the dead-time was not long enough to achieve full-ZVS [47]. The measurements of clamping-capacitor's voltage and primary current at 850 V are provided in Fig. 11 as well. One can see that maximum voltage of clamping capacitor is $\approx$8 V lower than the simulated one (Fig. 3). This is good because it is on a side of safety. Rest of the comments is similar to the ones for the operation at 620 V.

The efficiency curves of ACF in ACM are presented in Fig. 12. Maximum efficiencies in Fig. 12 were 84.5 % at 620 V and 81.2 % at 850 V. It is clear that the circulating-power losses are higher at higher input-voltage hence efficiency is lower [16], [23]. The reason for such not-so-high-efficiency in general is that the ACF circulating-power losses were high as well as dc-voltage-conversion-ratio.

B. OPERATION IN ICS STAND-BY MODE

Waveforms of gate- and drain-source voltages, primary current, and voltage of clamping capacitor at 640 V with load of 10.5 W are evaluated here. Those waveforms look similar for the ones at 460 V input—just with lower extremes. Hence, the 460 V ones are omitted here in order to avoid cluttering of the paper.

In Fig. 13 one can see relevant waveforms without hybrid-clamp. There one can read max QL drain-source (i.e. SW node) voltage of 1340 V. Moreover, one sees big ringing as a consequence of usage of external inductor, i.e. huge stored energy needed for ZVS in ACM. From Fig. 13 it is clear that the hybrid-clamp is a must for ACF with multi-mode control ICs in ICS applications.

In Fig. 14 the efficiency curves, at 460 V and 640 V, are presented. As expected, with higher input voltage the efficiency is lower. When compared with efficiency curves of 13 W ACF presented in [24] one can conclude that efficiency is lower in this case. That makes sense since the other ACF converter operated at its rated load in ACM, and the 57 W ACF here

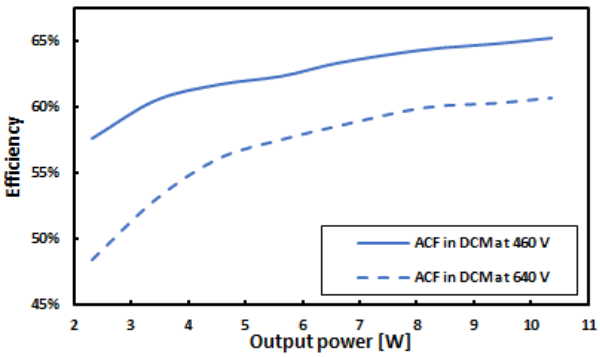

FIGURE 14. The efficiency of 57 W ACF operating in ICS stand-by mode (i.e. disabled-ACM).

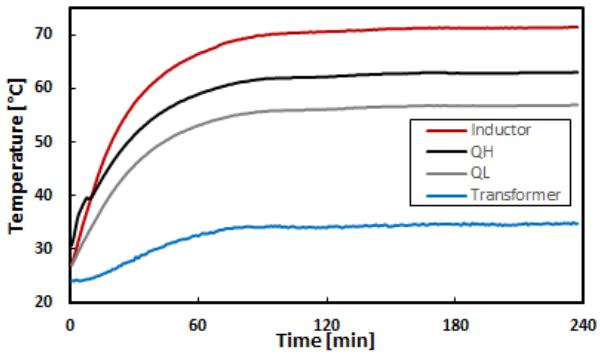

FIGURE 15. The long-term thermal test of 57 W ACF implemented in ICS and operating in ACM at 850 V dc link voltage.

operates at light load (i.e. disabled-ACM). The light-load in our case is <17 % of the rated one.

C. THERMAL MEASUREMENTS

The result of four-hours test of the implemented ACF in the ICS is shown in Fig. 15 [23]. The estimated load of ACF was around 40% because not all functions of the ICS were implemented. Furthermore, the ACF was a bit overdesigned in order to have a power reserve. Anyway, with such results one can expect that, with rated load and higher ambient temperature, maximum temperatures will be ≤110°C—which was the goal.

The ICS was completely enclosed (IP67) and had forced-cooling enabled during the test. Transformer, inductor, and switch QH were connected to the housing by thermal gap-pad for better conduction-cooling. Actually, this was disadvantage of the ACF in this application. The ambient temperature was around 25 °C. Results shown in Fig. 15 are satisfying. As expected, the inductor was the hottest part (71.4 °C) followed with QH. The thermal-camera screenshot of ACF implemented in demo-board is provided in [23].

D. ALTERNATIVE EFFICIENCY-GRAPHS

In Table 5 an overview of 10 different transformers, which were used during the study, is shown. It also provides data on

TABLE 5. Overview of the used ACF transformers.

Transformer: L_m, vendor	n	L_e [μH]	C_c [nF]
T1-1: 200 μH, vendor 1	10	47	88
T1-2: 200 μH, vendor 3	10	47	88
T1-3: 200 μH, vendor 3	15	47	88
T2-1: 400 μH, vendor 2	15	68	66
T2-2: 400 μH, vendor 3	15	68	66
T3-1: 600 μH, vendor 1	**15**	**100**	**88**
T3-2: 600 μH, vendor 2	15	100	88
T3-3: 600 μH, vendor 3	15	100	88
T4-1: 800 μH, vendor 1	15	100	66
T4-2: 800 μH, vendor 3	30	100	66

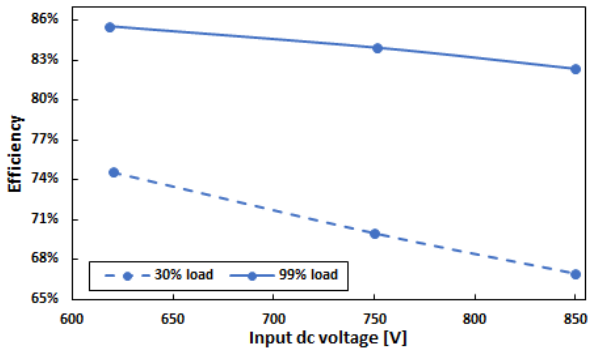

FIGURE 16. The 57 W ACF efficiency graph in ACM measured with constant load of 30 % and 99 %. Transformer T2-1 (Table 5) was used.

magnetizing inductance (L_m), turns ratio (n), and manually tuned resonant-tank (i.e. clamping capacitor and external inductor; C_c, L_e)—parameters which enabled highest efficiency for each case. The leakage inductance was made to be as low as possible ($\leq 9\,\mu$H) for all transformers and is not included in Table 5. All results presented in the paper so far were related to transformer T3-1 (Table 5 and Fig. 2). In this sub-section and in IV-E results with other transformers will be presented as well. The reasons for such approach were: a) one had to evaluate several vendors; b) due to limited budget a few parts were ordered of each transformer version; and c) during project execution (and parts usage) some of the samples were not available anymore hence one had to use what was at hand in our stock.

In Fig. 16 one can see dependency of ACF efficiency versus input dc voltage at constant loads of 30 % and 99 % with T2-1 transformer. If T3-1 would have been used in Fig. 16 then efficiencies would have been a bit lower (i.e. shifted down for ≈ 1–2 %). The graphs in Fig. 16 are almost linear and inverse-proportional to input voltage as expected. But one can see that, at smaller load, the efficiency line is steeper when input voltage is increased. The reason is that, at smaller loads, the switching and core losses, that are proportional to input voltage, are more dominant than the other losses. That explains why those two efficiency lines are not parallel.

The Fig. 17 presents dependency of ACF maximum efficiency versus magnetizing inductance. Those graphs are

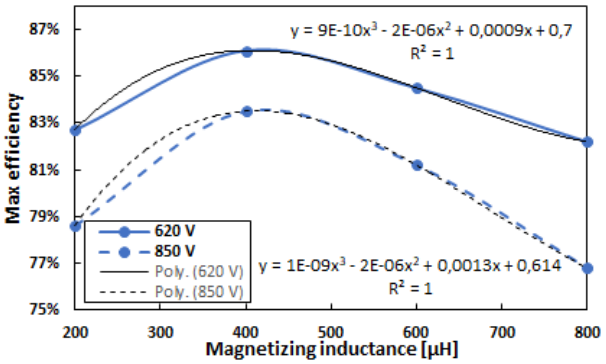

FIGURE 17. The 57 W ACF (hypothetical) maximum-efficiency graph in ACM measured with T1-1, T2-1, T3-2 and T4-1 transformers (Table 5). Blue lines: Microsoft® Excel® XY plots with smooth lines. Black lines: Microsoft® Excel® polynomial trend-lines.

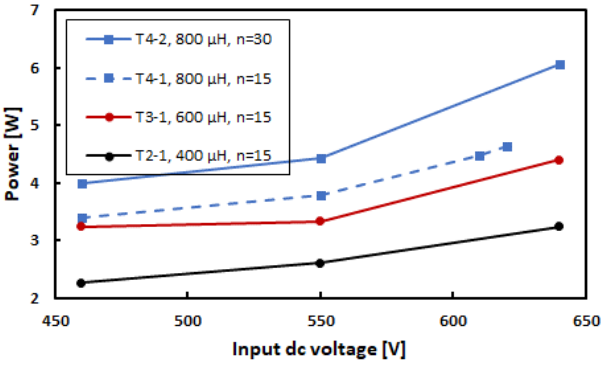

FIGURE 18. The 57 W ACF circulating-power losses measured with T2-1, T3-1, T4-1 and T4-2 transformers (Table 5).

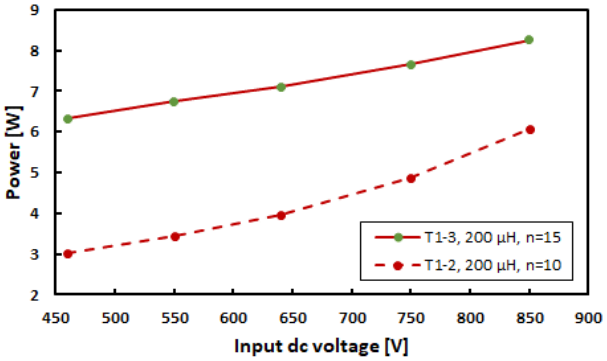

FIGURE 19. The 57 W ACF circulating-power losses measured with T1-2 and T1-3 transformers (Table 5).

hypothetical ones since they are created by taking maximum efficiencies of ACFs with four different transformers at two input dc voltages. The Fig. 17 clearly shows that ACF, specified in Table 2, will have maximum efficiencies (86.1 %; 83.5 %) if magnetizing inductance is around 400 μH with chosen turns-ratio and related resonant-tank parameters. In addition, one can notice that, at 850 V, losses are getting higher for other designs hence curves are not parallel but have different slopes too. Explanation for steeper slope at 850 V in inductances range 400–800 μH is similar as for Fig. 16. For inductances in range 200–400 μH steeper slope at 850 V is due to higher peak primary-currents hence associate losses. Additionally, in Fig. 17 polynomial curve-fitting lines are displayed. The polynomial curve-fitting function shows that maximum efficiency (η_{max}) has a weak cubic-dependency on the magnetizing inductance. However, whether such expression represents a real physical relationship will be investigated in a future paper together with analysis of accuracy and errors. However, it shall not be forgotten that efficiency is dependent on many other factors like transformer turns-ratio and its construction, resonant-tank parameters, choice of semiconductors, control methods, etc.

Note that in ICS the T3-1 is used (600 μH)—although maximum ACF efficiency was achieved for 400 μH in ACM (Fig. 17). Reason for such choice was that solution with 400 μH had higher peaks of SW-node voltages, when operating in ICS stand-by mode, so it was a bit risky to go with it. The detailed comparison of ACF efficiency curves (400 μH vs. 600 μH transformers) for different vendors one can find in [23].

E. NOTES ON CIRCULATING-POWER LOSSES

In Fig. 18 and Fig. 19 the "*circulating-power losses vs. input dc-voltage*" graphs, for six transformers and relevant resonant-tanks, are presented. This is the first paper on ACF where such results are presented. Those graphs were created with ACF under no-load condition (neglecting self-consumption and losses on bleeder resistors at outputs). The NCP1568 has possibility to set DCM to ACM transition thresholds with two resistors to ground (pin *6: DTH* and pin *13: ATH*) [32]. A document which describes how to force the NCP1568 to operate in DCM-only or ACM-only modes has to be requested from *onsemi application team* [39]. Because it is not publicly available it cannot be cited here. The ACF was first forced to operate in ACM only. Then the input power was measured with a precision power-analyzer. Next, the ACF was forced to operate in DCM-only (like conventional flyback converter). Then the input power was measured again with a precision power-analyzer. Difference between those input-powers provided the losses in active-clamping branch only, i.e. circulating-power losses in Fig. 18 and Fig. 19.

With transformers used in Fig. 18 it was possible to manually force ACF to operate in both modes (ACM and DCM) only up to 640 V. With higher voltages the DCM-only operation was possible. However, for T1-1 and T1-2, in Fig. 19, it was possible to make ACF operate in both modes up to 850 V. The reason for this probably lies in the way how the NCP1568 powers-up and later decides on threshold transitions. Moreover, in designs with T1-1 and T1-2 (200 μH) one gets highest peak-currents during start-up as well as in normal operation—when compared to the other transformer designs. Note that this IC, like all others for ACF in the market, was not created for such an application. Maybe here also partially

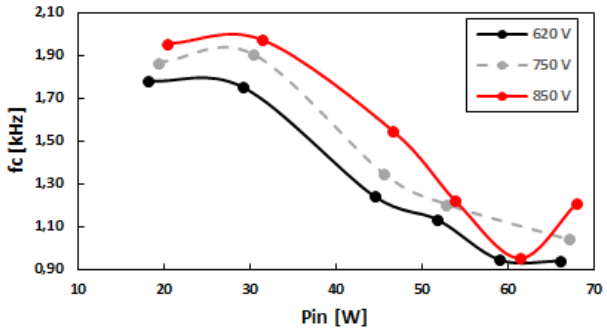

FIGURE 20. The 57 W ACF in ACM: the bandwidth (f_c) change with input voltage and input power.

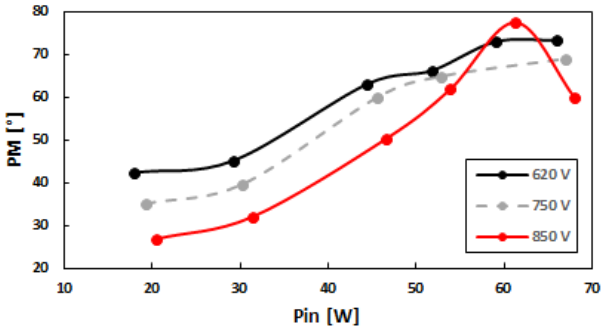

FIGURE 21. The 57 W ACF in ACM: the phase margin (PM) change with input voltage and input power.

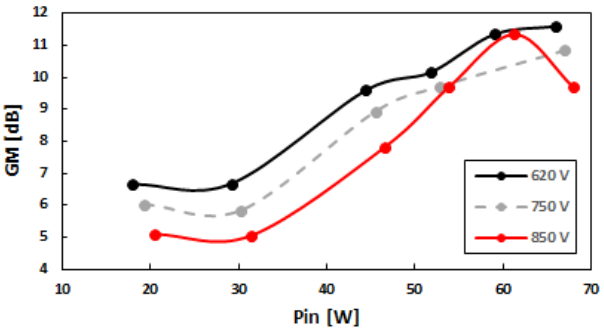

FIGURE 22. The 57 W ACF in ACM: the gain margin (GM) change with input voltage and input power.

lies the cause of that behavior. Hopefully those results will motivate vendors to create dedicated ACF control ICs for HDCIV applications in future.

In [14] and [27] is claimed that circulating-energy in complementary-switching case is higher than in the non-complementary one. This is correct since, in complementary-switching case, the turn-on time of QH is much longer than the QL one.

Only three papers so far were studying the circulating-energy in ACF [14], [20], and [27]. A detailed theoretical work is done for the non-complementary switching ACF in [14], for both DCM and CCM cases, as well as in [27] for the CCM case. The ACF with complementary switching in CCM was analyzed in [20] (e.g. *Fig. 9*, *Fig. 10* and *Table I*). It is clarified that, during C_c charging, losses are coming from conduction of QH freewheeling diode, i.e. average clamping-current matters [20]. But, during circulating-energy transfer to the secondary side, the losses are coming from QH conduction, i.e. rms value of clamping-current matters [20]. Derivation of appropriate mathematical expression for the circulating-power losses will be subject of a future study.

F. CONTROL ASPECTS

Although the ACF is known for around 30 years its small-signal analysis and modeling was subject of research only in last several years [17], [48]–[50]. The ACF in DCM ACM is combination of a PWM converter (during on-time) and a resonant one (during off-time) [49], [50]. This feature of ACF complicated its analysis and probably contributed to delay in research activities on small-signal analysis. Anyway, with [17], [48], [49], and [50] that topic is closed.

In all papers covering either small-signal modeling or compensator design the respective authors typically were presenting a few Bode diagrams, under key operating-conditions, and dynamic load-change in order to prove the effectiveness of their proposed methods. However, graphical representation of bandwidth (f_c), phase-margin (PM), and gain-margin (GM) changes in whole load-range was missing. Hence, in Fig. 20, Fig. 21, and Fig. 22 such graphs are presented for the first time in literature on the ACF control.

The Bode plots of 57 W ACF operating in DCM ACM, with T2-2 transformer, were measured with *Bode 100* vector network-analyzer [51]. Excitation signal was 20 mV (peak-to-peak). From those plots, for each measured operation point, the cross-over frequency, PM, and GM are extracted. And, results are plotted in Fig. 20, Fig. 21, and Fig. 22. Those quantities are plotted vs. input power because that was much faster to do rather than calculating output power by measuring load at five outputs. Operation at six loads and three input voltages were measured. Note that all taken Bode plots had first-order response that is typical for a peak-current controlled flyback dc-dc converter [30].

The compensator used was the ATL431 [52] based Type-2 (integrator, one pole and one zero) one with an opto-coupler. Its key-parameters were dc-gain of 34.1 dB, zero at 8.8 Hz, and pole at 4.97 kHz. The parameters of compensator were first calculated then verified by simulations and in the lab. The used opto-coupler had minimum current-gain of 1.6 and estimated parasitic capacitance of ≈3 nF.

In Fig. 20, Fig. 21, and Fig. 22 one can see that all three quantities are changeable with load and input voltage—which was expected. The point at 850 V and 61.3 W is not a mistake, i.e. it is plausible. That was confirmed by repeating measurements on a different day with different excitation signal (30 mV, peak-to-peak). From practical experience, the PM shall be $>35°$ and GM$>$6 dB for all operating conditions. We see that is only fulfilled for operation at 620 V. However,

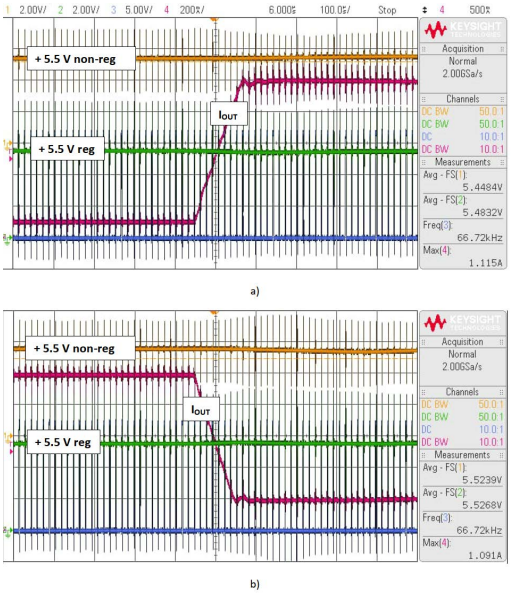

FIGURE 23. The 57 W ACF in ACM with dynamic load-change at +5.5 V regulated output. Another +5.5 V non-regulated output had load of 1 A. a) current change from 0.1 A to 1 A; b) current change from 1 A to 0.1 A.

in ICS power-transfer mode, the ACF will operate in ACM because its input power will be higher than 30 W. This means that no stability problems with input voltages higher than 750 V are expected. Additionally, the bandwidth was in 0.9–2 kHz range which was good. It is worth mentioning that the resulting bandwidth is less than 1/30 f_{sw_min}. Note that in a common engineering practice on power-converters' control it is usually advised to have $f_c < 1/10\, f_{sw\_min}$.

The dynamic load change at +5.5 V regulated output (10 % to 100 % and vice versa) is presented in Fig. 23. There one can see that the designed compensator is working as expected with overshoots and undershoots less than ±5.5 %. Those results were acceptable for our application. The signal-noise visible in Fig. 23 is result of the pick-up by used probes, i.e. it is not a problem within the converter itself.

G. COMPARISON TO CONVENTIONAL DCM FLYBACK

The ACF was easily modified into conventional DCM flyback converter by simply disabling QH gate-signals, shorting inductor, and adjusting resistors' values in the clamping circuit. Advantage of this method was that one had the same control IC, transformer, and rest of the circuitry. Hence difference in losses came only from the disabled active-clamping branch. Main focus of this comparison was on efficiency, price and occupied board-space. The comparison of control-aspects to an ACF will be studied in a future paper.

In Fig. 24 one can see the difference in efficiency. The used transformer was T2-2 (0.4 mH) and it was evaluated in [23] under the name "*T2*". As expected, the DCM flyback had higher efficiency in lower load-range. Only at loads >29 W (i.e. >50 %) the efficiencies were similar. This shows that

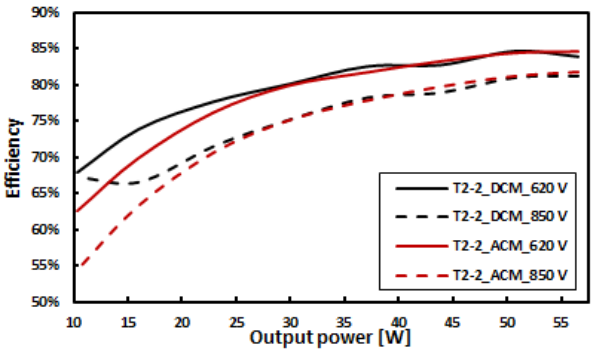

FIGURE 24. The DCM flyback vs ACF efficiencies with T2-2.

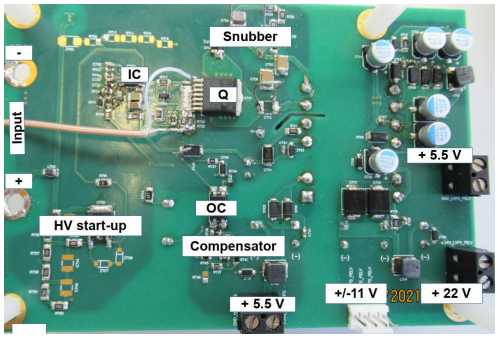

FIGURE 25. The QRF prototype (demo) board (top view).

HDCIV ACF would be more suitable for power levels higher than 60 W.

By simply comparing bill-of-material and considering cheaper control IC without high-side driver, it is calculated that conventional DCM flyback is roughly 23 % cheaper than the ACF. Additionally, the ACF occupies ≈11 % more board-space than the DCM flyback thus increasing costs further. So, if the ACF efficiency is much lower than the DCM flyback one—the only reason why to use the ACF might be due to reduced EMI [26] in applications that are not cost-sensitive [24], but where EMI concern is high (like ICS).

H. COMPARISON TO QUASI-RESONANT FLYBACK

The QRF converter is designed as a separate one having the same specification as ACF (including transformer). It used the same SiC FET as in the ACF [43]. This made comparison of ACF and QRF easier and more plausible. The photo of QRF demo-board is given in Fig. 25. It had the same dimensions as the ACF one (9x13 cm).

For its control the *onsemi* device NCP1340 [53] was used. This is multi-mode controller with adaptive switching- frequency. Main focus of this comparison was on efficiency, price and occupied board-space. The detailed evaluation of the QRF in ICS application, including control-aspects, and comparison to ACF control, will be subject of a future paper.

The QRF is more suitable for HDCIV use than DCM flyback due to valley-switching, hence reduced switching losses. In Fig. 26 one can see the difference in efficiencies

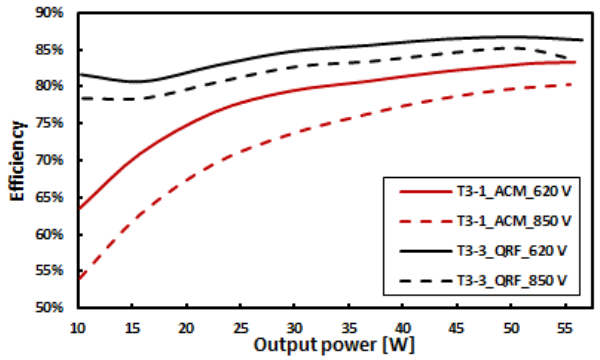

FIGURE 26. The QRF vs ACF efficiencies with T3-1 and T3-3.

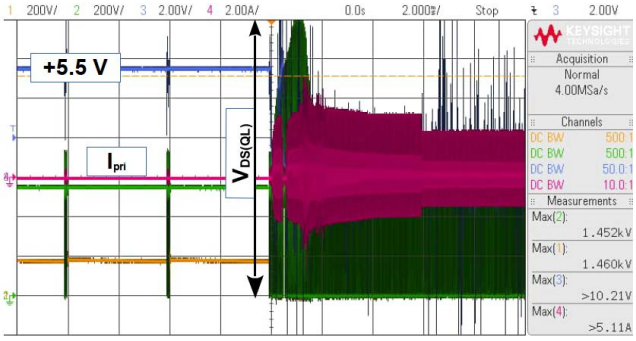

FIGURE 27. The 57 W ACF in pulse-skipping mode (zero-load) at 550 V input. The short-circuit is applied at t = 0 on +5.5 V regulated output.

between ACF and QRF. As expected, the QRF had higher efficiency in whole load range. Note that vendors of transformers for ACF and QRF were different. Due to different transformers' availability in different project stages the ACF used the T3-1 one whereas QRF used the T3-3 one. The T3-3 design was a bit worse, in terms of losses, than the T3-1 one. Hence, one would get some small increase in the efficiency for QRF in Fig. 26 if one would use the T3-1 transformer instead of T3-3. In addition, the QRF operated with variable switching-frequencies ≤ 50 kHz. This also contributed to slightly higher efficiency than the ACF—which was always working with frequencies ≥ 66 kHz. However, both contributions to efficiency-difference cannot overcome the fact that ACF had high circulating-power losses.

Regarding price difference the QRF is roughly 23 % cheaper than the ACF. Additionally, the ACF occupies $\approx$11 % more board-space than the QRF thus increasing costs further. Therefore, if the ACF efficiency is much lower than the QRF one—the only reason why to use the ACF might be due to reduced EMI [26] in applications that are not cost-sensitive [24], but where EMI concern is high (like ICS). This is the same conclusion that is reached for the DCM flyback case.

I. ACF SHORT-CIRCUIT BEHAVIOUR

The protection against short-circuit at output is a crucial part of design of any dc-dc converter. Hence, ACF is not an exception and its chosen controller [32]. That controller is a peak-current controlled IC, so it is easy to achieve the peak-current limitation. Evaluation of ACF short-circuit behavior is analyzed for the first time in literature. The ACF was tested with short-circuit, at its outputs, in following cases:

1) Regulated output +5.5 V shorted during power-up;
2) Regulated output +5.5 V shorted during operation in ACM;
3) Non-regulated output +22 V (with biggest load) shorted during power-up;
4) Non-regulated output +22 V (with biggest load) shorted during operation in ACM.
5) Regulated output +5.5 V shorted during operation in DCM (disabled-ACM).

The ACF passed tests 1–4 without any problems. The peak-current was limited, and ACF attempted auto-restart after predefined time of 1.6 s [32] (i.e. kind of hiccup mode).

However, it turned out that the multi-mode ACF is most vulnerable if short-circuit would have happen during pulse-skipping or DCM operation (i.e. disabled-ACM) without hybrid-clamp. This is another reason why hybrid-clamp is a must for a multi-mode ACF. In Fig. 27 one can see the ACF waveforms during short-circuit at regulated output +5.5 V in pulse-skipping mode without hybrid-clamp. From Fig. 27 one sees that maximum drain-source voltage (i.e. SW node) was going up to 1452 V with 550 V input.

Note that during short-circuit contact-bouncing (<2 ms) of the external switch was noticeable. This is visible on +5.5 V waveform in Fig. 27 but had no influence on conclusions. Hence, to make ACF more robust in HDCIV applications one needs hybrid-clamp plus better half-bridge drivers, and bootstrap diodes. It is not clear whether protection features in ACF control ICs for ICS could be improved since protection against short-circuit was already implemented [32], [33].

V. LIMITATIONS AND FUTURE WORK

A. LIMITATIONS OF THE STUDY

Every study has limitations—even if not openly stated—hence this one is not an exception. As already mentioned in sub-section I-A, this work was part of a commercial project. Therefore, the project-timeline had higher priority over applied-research activities. Hence, sometimes one had to use trial-and-error approach to find a good-enough solution and move-on. There was no time for complicated mathematics or for development of dedicated optimization algorithms. Other limitations are:

- The APS in any commercial device has to operate standalone, i.e. one had to use an analog-control IC. With this approach the control method is fixed, i.e. there was no freedom to use custom-made analog or digital control which might get some advantages. However, the NCP1568 is state-of-the-art ACF control IC with modern features [32].
- The APS had to be realized as one stage due to board-space limitation and cost-reduction. This led to

high dc-voltage-conversion-ratio [23], [24], and low ACF efficiency. Hence some components had higher temperatures and had to be cooled. For example, one could get better ACF performance with two dc-dc stages in cascade—with ACF being the latter stage, having fixed input voltage and reduced number of outputs.
- Some of the formulas are derived by curve-fitting of the experimental curves.
- Usage of the ACF in HDCIV application (i.e. ICS) is a pioneering work. Hence there was no appropriate literature available or, sometimes, even no appropriate support from the parts' vendors.
- A balance between practical and academic contributions is tried to be achieved. However, target audience is more in direction of development engineers, PhD students, and manufacturers of electronic components.

B. FUTURE WORK

Authors' wish is that this study influences manufacturers of electronic components to develop better ones tailored for the HDCIV application. That would enable the ACF to be more utilized in that market segment—especially in an emerging one like the ICS.

Moreover, some challenges or questions emerged during this study but remained unsolved or unanswered. Some of them are left in such status on purpose in order to avoid that this paper gets too big. We hope that fellow researches would get inspired to tackle some of the items listed below. Some possibilities for future work are:

- Develop optimization method for the transformer design and overall power stage.
- Optimize or automate the control-loop design for multi-output ACF with two operating modes (ACM and DCM), two loading conditions, and two input-voltage ranges. In the reviewed literature so far an optimization algorithm for controller design was used only in [25] and [54].
- Compare control aspects of ACF vs. conventional DCM flyback converter and ACF vs. QRF in HDCIV application.
- Further evaluate results presented in Fig. 17–Fig. 19, develop mathematical expressions for them, and include error-analysis.

VI. SUMMARY AND CONCLUSION

This paper presented investigation of ACF dc-dc converter 57 W used as APS of an ICS for EV. Since the ACF was supplied from HDCIV that created additional challenges for its design which are different from mainstream ACF applications. However, some findings and conclusions are applicable to any ACF converter.

First, an overview of the ACF control ICs is given. It was obvious that their target applications were single-phase ones (i.e. for consumer electronics) and not the HDCIV one. Only two vendors so far had devices that can be used for the ICS application, but external HV start-up circuit is needed. Then, the ACF with two input-voltage ranges and two loads, with different loading of outputs, was investigated. The choice of magnetizing inductance in such case is explained. That approach is applicable to any kind of flyback converters.

As next, the challenges of key-components' choice were presented. The power switch (SiC 1700 V), half-bridge driver with accompanied bootstrap diode, and external inductor (needed for ZVS) are all single-source parts. This is not desirable for the mass-production. Some notes are given on preferred features. In addition, updated suggestion of control IC features (from [23]) is presented.

Furthermore, choice of clamping capacitor is explained, and several formulas are compared. It was shown that, after verification in the lab, only one formula was useful. Additionally, need of usage of hybrid-clamp for ACF with multi-mode control IC is explained in detail as well as short-circuit behavior of the ACF.

Some notes are given for ZVS operation together with table of energies stored in resonant-tank elements. Such table is, for the first time, presented for an ACF converter. Since resonant inductance is not negligible, when compared to the magnetizing one, one had to correct conventional expression for calculation of the flyback switching-node voltage.

The simulation of basic waveforms is done in SIMPLIS and results were well matched with the measured ones. The efficiency is investigated in detail and it was shown that it is not as high as reported for ACF in mainstream applications. The reasons for that are high circulating-power losses and high dc-voltage-conversion-ratio. However, the graph of hypothetical "*maximum efficiency vs. magnetizing inductance*" is shown for the first time. The maximum efficiency of 86.1 % was achieved at $\approx$400 μH and 620 V input with resonant-tank parameters of 66 nF and 68 μH (no leakage-inductance included). Work in this area might be continued.

The investigation of circulating-power losses is done for six different transformers. The graphs of "*circulating-power losses vs. input voltage*" are shown for the first time. It was seen that they are huge (i.e. several watts) and that they increase with input voltage. Work in this area will be continued.

Thermal tests showed that cooling of QH and inductor was needed—which is a drawback and not desired for a mass-production. However, several systems with ACF as the APS work seamlessly so far.

At the end, a comparison of ACF with conventional DCM flyback and QRF converters was done. Conclusion for both was that they are $\approx$23 % cheaper, occupy $\approx$11 % less board-space and have higher or equal efficiencies depending on load conditions. However, efficiency itself is not a key-feature of a converter that is used as an APS as long as there are no thermal problems. Knowing that ACF has lower EMI [26] than conventional flyback converters could be the key advantage in emerging application like ICS for EV.

In order to make ACF performances better in HCD-CIV application and promote its wider usage it is needed

that vendors of electronic components develop better or second-source devices targeting ICS market-segment.

In section V the study-limitations and opportunities for future work on ACF are listed. Further work is planned on both ACF and QRF converters for ICS.

VII. CONFLICT OF INTEREST DECLARATION

Authors declare no conflict of interests that could have influenced the work reported in this paper and do not endorse any manufacturer of electronics components.

ACKNOWLEDGMENT

The authors thank onsemi for providing samples of the NCP1568 control IC and for technical support; United Silicon Carbide Inc. for providing samples of the 1700 V SiC FETs, and Zöllner Elektronik AG for technical support.

Support from management of Brusa Elektronik (München) GmbH, ex-colleagues Dr. M. Pavlovský and Dr. R. Ruffo, and other colleagues is highly appreciated.

Authors are fond of free and open-source software. Hence, they would like to give credits to the people who created those programs. Some of the figures were made or edited by using FidoCADJ [55], GNU Octave [56] and Libre Office Draw [57]. The references were managed in Zotero [58].

REFERENCES

[1] A. Ahmad, M. S. Alam, and R. Chabaan, "A comprehensive review of wireless charging technologies for electric vehicles," *IEEE Trans. Transport. Electrific.*, vol. 4, no. 1, pp. 38–63, Mar. 2018, doi: 10.1109/TTE.2017.2771619.

[2] D. Patil, M. K. McDonough, J. M. Miller, B. Fahimi, and P. T. Balsara, "Wireless power transfer for vehicular applications: Overview and challenges," *IEEE Trans. Transport. Electrific.*, vol. 4, no. 1, pp. 3–37, Mar. 2018, doi: 10.1109/TTE.2017.2780627.

[3] H. Feng, R. Tavakoli, O. C. Onar, and Z. Pantic, "Advances in high-power wireless charging systems: Overview and design considerations," *IEEE Trans. Transport. Electrific.*, vol. 6, no. 3, pp. 886–919, Sep. 2020, doi: 10.1109/TTE.2020.3012543.

[4] S. Li and C. C. Mi, "Wireless power transfer for electric vehicle applications," *IEEE J. Emerg. Sel. Topics Power Electron.*, vol. 3, no. 1, pp. 4–17, Mar. 2015, doi: 10.1109/JESTPE.2014.2319453.

[5] A. El-Shahat, E. Ayisire, Y. Wu, M. Rahman, and D. Nelms, "Electric vehicles wireless power transfer state-of-the-art," *Energy Proc.*, vol. 162, pp. 24–37, Apr. 2019, doi: 10.1016/j.egypro.2019.04.004.

[6] T. M. Fisher, K. B. Farley, Y. Gao, H. Bai, and Z. T. Tse, "Electric vehicle wireless charging technology: A state-of-the-art review of magnetic coupling systems," *Wireless Power Transf.*, vol. 1, no. 2, pp. 87–96, Sep. 2014, doi: 10.1017/wpt.2014.8.

[7] BRUSA Elektronik AG. Accessed: Feb. 28, 2022. [Online]. Available: https://www.brusa.biz

[8] K. Yoshida, T. Ishii, and N. Nagagata, "Zero voltage switching approach for flyback converter," in *Proc. 14th Int. Telecommun. Energy Conf. (INTELEC)*, Washington, DC, USA, 1992, pp. 324–329, doi: 10.1109/INTLEC.1992.268424.

[9] R. Watson, F. C. Lee, and G. C. Hua, "Utilization of an active-clamp circuit to achieve soft switching in flyback converters," *IEEE Trans. Power Electron.*, vol. 11, no. 1, pp. 162–169, Jan. 1996, doi: 10.1109/63.484429.

[10] X. Huang, J. Feng, W. Du, F. C. Lee, and Q. Li, "Design consideration of MHz active clamp Flyback converter with GaN devices for low power adapter application," in *Proc. IEEE Appl. Power Electron. Conf. Expo. (APEC)*, Long Beach, CA, USA, Mar. 2016, pp. 2334–2341, doi: 10.1109/APEC.2016.7468191.

[11] L. Xue and J. Zhang, "Highly efficient secondary-resonant active clamp flyback converter," *IEEE Trans. Ind. Electron.*, vol. 65, no. 2, pp. 1235–1243, Feb. 2018, doi: 10.1109/TIE.2017.2733451.

[12] A. Zaman and A. Radic, "How to design and implement an adapter power supply with active clamp flyback: An all silicon design methodology," *IEEE Power Electron. Mag.*, vol. 7, no. 4, pp. 36–43, Dec. 2020, doi: 10.1109/MPEL.2020.3033608.

[13] B.-R. Lin, H.-K. Chiang, K.-C. Chen, and D. Wang, "Analysis, design and implementation of an active clamp flyback converter," in *Proc. Int. Conf. Power Electron. Drives Syst.*, Kuala Lumpur, Malaysia, 2005, pp. 424–429, doi: 10.1109/PEDS.2005.1619724.

[14] J. Zhang, X. Huang, X. Wu, and Z. Qian, "A high efficiency flyback converter with new active clamp technique," *IEEE Trans. Power Electron.*, vol. 25, no. 7, pp. 1775–1785, Jul. 2010, doi: 10.1109/TPEL.2010.2042302.

[15] P.-H. Liu, "Design consideration of active clamp flyback converter with highly nonlinear junction capacitance," in *Proc. IEEE Appl. Power Electron. Conf. Expo. (APEC)*, San Antonio, TX, USA, Mar. 2018, pp. 783–790, doi: 10.1109/APEC.2018.8341101.

[16] P. Alou, O. Garcia, J. A. Cobos, J. Uceda, and M. Rascon, "Flyback with active clamp: A suitable topology for low power and very wide input voltage range applications," in *Proc. 17th Annu. IEEE Appl. Power Electron. Conf. Expo. (APEC)*, Dallas, TX, USA, Mar. 2002, pp. 242–248, doi: 10.1109/APEC.2002.989254.

[17] S. Xu, Q. Qian, R. Shi, S. S. Shah, Q. Liu, S. Lu, and W. Sun, "Sampled-data modeling for PCM and ZVS controlled critical conduction mode (CrCM) active clamp flyback (ACF) converter at variable switching frequency," *IEEE Trans. Circuits Syst. I, Reg. Papers*, vol. 67, no. 10, pp. 1–13, Oct. 2020, doi: 10.1109/TCSI.2020.2993256.

[18] S. Ben-Yaakov. (2018). *Deciphering Flyback Converters Active Clamps*. Accessed: Jan. 9, 2022. [Online]. Available: https://www.youtube.com/watch?v=ySC-SvoQa3U

[19] R. Perrin, N. Quentin, B. Allard, C. Martin, and M. Ali, "High-temperature GaN active-clamp flyback converter with resonant operation mode," *IEEE J. Emerg. Sel. Topics Power Electron.*, vol. 4, no. 3, pp. 1077–1085, Sep. 2016, doi: 10.1109/JESTPE.2016.2544346.

[20] Q. Zhao, F. Tao, Y. Hu, and F. C. Lee, "Active-clamp DC/DC converters using magnetic switches," in *Proc. 16th Annu. IEEE Appl. Power Electron. Conf. Expo. (APEC)*, Anaheim, CA, USA, Mar. 2001, pp. 946–952, doi: 10.1109/APEC.2001.912481.

[21] A. Nasiri and A. S. Saadat Abadi, "A new driving method for a magnetron using a soft switching active clamp fly-back converter," in *Proc. 10th Int. Power Electron., Drive Syst. Technol. Conf. (PEDSTC)*, Shiraz, Iran, Feb. 2019, pp. 361–366, doi: 10.1109/PEDSTC.2019.8697583.

[22] A. Nasiri, M. R. Banaei, and A. S. S. Abadi, "Phase-shifted active clamp flyback converter for driving a magnetron," in *Proc. 27th Iranian Conf. Electr. Eng. (ICEE)*, Yazd, Iran, Apr. 2019, pp. 2106–2110, doi: 10.1109/IranianCEE.2019.8786649.

[23] D. Vračar and M. Pavlovský, "Implementation of active-clamped flyback DC-DC converter in an 800 V system," in *PCIM Eur. Digit. Days*, 2021, pp. 1163–1170. [Online]. Available: https://ieeexplore.ieee.org/document/9472384

[24] D. D. Vracar, M. Pavlovsky, and P. Pejovic, "Active-clamped fly-back DC-DC converter in three-phase application," in *Proc. 21st Int. Symp. Power Electron. (Ee)*, Novi Sad, Serbia, Oct. 2021, pp. 1–6, doi: 10.1109/Ee53374.2021.9628263.

[25] C. T. Choi, C. K. Li, and S. K. Kok, "Control of an active clamp discontinuous conduction mode flyback converter," in *Proc. IEEE Int. Conf. Power Electron. Drive Syst. (PEDS)*, Hong Kong, Jul. 1999, pp. 1120–1123, doi: 10.1109/PEDS.1999.792865.

[26] X. Huang, J. Feng, F. C. Lee, Q. Li, and Y. Yang, "Conducted EMI analysis and filter design for MHz active clamp flyback front-end converter," in *Proc. IEEE Appl. Power Electron. Conf. Expo. (APEC)*, Long Beach, CA, USA, Mar. 2016, pp. 1534–1540, doi: 10.1109/APEC.2016.7468071.

[27] K.-S. Kim, S.-H. Lee, W.-J. Cha, J.-M. Kwon, and B.-H. Kwon, "Bidirectional single power-conversion DC–AC converter with noncomplementary active-clamp circuits," *IEEE Trans. Ind. Electron.*, vol. 63, no. 8, pp. 4860–4867, Aug. 2016, doi: 10.1109/TIE.2016.2550021.

[28] L. Huber, M. M. Jovanovic, H. Song, D. Xu, A. Zhang, and C.-C. Chang, "Flyback converter with hybrid clamp," in *Proc. IEEE Appl. Power Electron. Conf. Expo. (APEC)*, San Antonio, TX, USA, Mar. 2018, pp. 2098–2103, doi: 10.1109/APEC.2018.8341306.

[29] Y. T. Yau, W. Z. Jiang, and K. I. Hwu, "Light-load efficiency improvement for flyback converter based on hybrid clamp circuit," in *Proc. IEEE Int. Conf. Ind. Technol. (ICIT)*, Taipei, Taiwan, Mar. 2016, pp. 329–333, doi: 10.1109/ICIT.2016.7474773.

[30] C. Basso, *Switch-Mode Power Supplies: Spice Simulations and Practical Designs*, 2nd ed. New York, NY, USA: McGraw-Hill, 2014.
[31] M. K. Kazimierczuk, *Pulse-Width Modulated DC-DC Power Converters*, 2nd ed. Hoboken, NJ, USA: Wiley, 2015.
[32] (Aug. 2021). Datasheet. *NCP1568: AC-DC active clamp Flyback PWM IC*. Onsemi. Accessed: Dec. 28, 2021. [Online]. Available: https://www.onsemi.com/pdf/datasheet/ncp1568-d.pdf
[33] (Feb. 2018). Datasheet. *UCC28780: High Frequency Active Clamp Flyback Controller*. TI. Accessed: Dec. 29, 2021. [Online]. Available: https://www.ti.com/lit/gpn/ucc28780
[34] Product Brief. *SZ1130: Flyback PWM Controller With Integrated Active Clamp Circuit*. Silanna Semi, Rev. 3.0. Accessed: Dec. 29, 2021. [Online]. Available: https://powerdensity.com/sz1110-sz1130-new/
[35] A. K. Hari and B. McCoy, "Switched mode power supply with efficient operation at light loads and method therefor," U.S. Patent 9 991 800 B2, Jun. 5, 2018. [Online]. Available: https://patents.google.com/patent/US9991800
[36] (Jan. 2021). Datasheet (Product Preview). *NCP1568D: DC-DC Active Clamp Flyback PWM IC*. Onsemi. Accessed: Dec. 29, 2021. [Online]. Available: https://www.onsemi.com/pdf/datasheet/ncp1568d-d.pdf
[37] (May 2021). Datasheet. *UCC28782: High-Density Flyback Controller for Active-Clamp (ACF) and Zero-Voltage Switching (ZVS) Topologies*. Accessed: Dec. 29, 2021. [Online]. Available: https://www.ti.com/lit/gpn/ucc28782
[38] (Nov. 2020). Datasheet. *ClampZero Family*. Power Integrations. Accessed: Dec. 29, 2021. [Online]. Available: http://powerint.com/downloads/documents/clampzero-data-sheet.pdf
[39] *E-mail—Private Communication*, Onsemi Application Team USA, Phoenix, AZ, USA, 2020.
[40] (Oct. 2021). White Paper. *High-Density AC–DC Power Supplies Using Active–Clamp Flyback Topology*. Onsemi. Accessed: Dec. 29, 2021. [Online]. Available: https://www.onsemi.com/pub/collateral/tnd6279-d.pdf
[41] *Safety of Transformers, Reactors, Power Supply Units and Combinations There of—Part 1: General Requirements and Tests*, Standard IEC 61558-1:2017, 2017. [Online]. Available: https://webstore.iec.ch/publication/26261
[42] A. B. Nadler, A. L. F. Stein, and C. R. Sullivan, "Transformer and frequency optimization in a GaN-based active-clamp flyback converter," in *Proc. IEEE Appl. Power Electron. Conf. Expo. (APEC)*, New Orleans, LA, USA, Mar. 2020, pp. 2709–2714, doi: 10.1109/APEC39645.2020.9124050.
[43] *UF3C170400B7S, 1700 V, SiC FET*, Datasheet (Preliminary), UnitedSiC. sales@unitedsic.com, USA, 2019.
[44] J.-H. Jung and S. Ahmed, "Low standby power consumption and high cross regulation of active clamp flyback converter with SSPR," in *Proc. 36th Annu. Conf. IEEE Ind. Electron. Soc. (IECON)*, Glendale, AZ, USA, Nov. 2010, pp. 544–549, doi: 10.1109/IECON.2010.5675224.
[45] S. Tang, J. Xi, and L. He, "A GaN-based MHz active clamp flyback converter with adaptive dual edge dead time modulation for AC-DC adapters," in *Proc. 43rd Annu. Conf. IEEE Ind. Electron. Soc. (IECON)*, Beijing, China, Oct. 2017, pp. 546–553, doi: 10.1109/IECON.2017.8216096.
[46] Software (Commercial). *SIMetrix/SIMPLIS ver. 8.50*. Accessed: 2021. [Online]. Available: https://www.simplistechnologies.com
[47] T. LaBella, B. York, C. Hutchens, and J.-S. Lai, "Dead time optimization through loss analysis of an active-clamp Flyback converter utilizing GaN devices," in *Proc. IEEE Energy Convers. Congr. Expo. (ECCE)*, Raleigh, NC, USA, Sep. 2012, pp. 3882–3889, doi: 10.1109/ECCE.2012.6342304.
[48] P.-H. Liu, "Small signal analysis of active clamp flyback converters in transition mode and burst mode," in *Proc. IEEE Appl. Power Electron. Conf. Expo. (APEC)*, Anaheim, CA, USA, Mar. 2019, pp. 241–248, doi: 10.1109/APEC.2019.8722081.
[49] S. Xu, Q. Qian, B. Ren, and Q. Liu, "An accurate small signal modeling and control loop design of active clamp flyback converter," in *Proc. 10th Int. Conf. Power Electron. ECCE Asia (ICPE-ECCE Asia)*, Busan, South Korea, May 2019, pp. 3259–3264, doi: 10.23919/ICPE2019-ECCEAsia42246.2019.8797022.
[50] S. Xu, Q. Qian, T. Tao, S. Lu, and W. Sun, "Small signal modeling and control loop design of critical conduction mode active clamp flyback converter," *IEEE Trans. Power Electron.*, vol. 36, no. 6, pp. 7250–7263, Jun. 2021, doi: 10.1109/TPEL.2020.3040451.
[51] (2019). Quick Start Guide. *Bode 100 Vector Network Anlyzer*. OMICRON Lab. [Online]. Available: https://www.omicron-lab.com
[52] (Oct. 2016). Datasheet. *ATL431, ATL432 2.5-V Low Iq Adjustable Precision Shunt Regulator*. Accessed: Mar. 19, 2022. [Online]. Available: https://www.ti.com/lit/gpn/atl431
[53] (Mar. 2021). Datasheet. *NCP1340: Quasi-Resonant Controller, High-Voltage, Featuring Valley Lock-Out Switching*. Onsemi. Accessed: Dec. 30, 2021. [Online]. Available: https://www.onsemi.com/pdf/datasheet/ncp1340-d.pdf
[54] C. T. Choi, C. K. Li, and S. K. Kok, "Modeling of an active clamp discontinuous conduction mode flyback converter under variation of operating conditions," in *Proc. IEEE Int. Conf. Power Electron. Drive Syst. (PEDS)*, Hong Kong, Jul. 1999, pp. 730–733, doi: 10.1109/PEDS.1999.792795.
[55] Software (Free). *FidoCadJ—A Free Graphical Editor for Electronics, Ver. 0.2.47*. Accessed: 2021. [Online]. Available: https://darwinne.github.io/FidoCadJ/
[56] Software (Free). *GNU Octave—A High-Level Interactive Language for Numerical Computations, ver. 6.2.0*. Accessed: 2021. [Online]. Available: https://www.gnu.org/software/octave/
[57] Software (Free). *Libre Office Draw, ver. 6.2.5.x*. Accessed: 2021. [Online]. Available: https://www.libreoffice.org
[58] Software (Free). *Zotero ver. 5.0.x.x*. Accessed: 2021. [Online]. Available: https://www.zotero.org

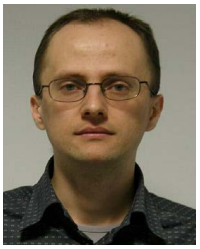

DARKO Đ. VRAČAR (Member, IEEE) was born in Ključ Bosnia and Herzegovina. He received the Dipl.-Ing. and Magister degrees in electrical engineering from the School of Electrical Engineering, University of Belgrade, Serbia, in 2000 and 2007, respectively, where he is currently pursuing the Ph.D. degree. His major field of study was power converters and drives.

He is also a Senior Staff Engineer with BRUSA Elektronik (München) GmbH, Munich, Germany. He has 21 years of industrial experience. Some areas of expertise are implementation of telecom and datacenter power supplies, and research and development of power electronics' systems, such as solar inverters, SMPS for industrial, automotive, and telecom applications. He has published several articles related to power converters and drives and holds one patent in power conversion systems. His research interests include simulation, control, and design of power converters. In addition, he was delivering training sessions related to power electronics or industrial standards.

Mr. Vračar is a member of the following IEEE Societies: Industry Applications, Industrial Electronics and Power Electronics. He is a Reviewer of journal *Electronics*.

PREDRAG V. PEJOVIĆ (Senior Member, IEEE) was born in Belgrade, Serbia, in 1966. He received the Dipl.-Ing. and Magister degrees in electrical engineering from the University of Belgrade, Serbia, in 1990 and 1992, respectively, and the Ph.D. degree from the University of Colorado, Boulder, CO, USA, in 1995.

He rejoined the University of Belgrade, in 1995, where he is currently a Professor in charge of teaching electrical measurements, software tools in electronics, analog electronics, and two courses in power electronics. His research interests include analog circuit design, three-phase high-power factor rectifiers, dynamics of nonlinear systems, electronic measurements, automated measurement systems, wireless positioning, and techniques for computer-aided analysis, design, and optimization of power electronic systems.